Biochemical and Biophysical Research Communications 455 (2014) 339–346

Contents lists available at ScienceDirect

Biochemical and Biophysical Research Communications

journal homepage: www.elsevier.com/locate/ybbrc

Structural and biochemical characterizations of an intramolecular tandem coiled coil protein

Donghyuk Shin [a], Gwanho Kim [a], Gyuhee Kim [a], Xu Zheng [b], Yang-Gyun Kim [b], Sangho Lee [a,*]

[a] Department of Biological Sciences, Sungkyunwan University, Suwon, Republic of Korea
[b] Department of Chemistry, Sungkyunwan University, Suwon, Republic of Korea

ARTICLE INFO

Article history:
Received 28 October 2014
Available online 15 November 2014

Keywords:
Coiled coil
Solution structure
Small-angle X-ray scattering
Ionic strength

ABSTRACT

Coiled coil has served as an excellent model system for studying protein folding and developing protein-based biomaterials. Most designed coiled coils function as oligomers, namely intermolecular coiled coils. However, less is known about structural and biochemical behavior of intramolecular coiled coils where coiled coil domains are covalently linked in one polypeptide. Here we prepare a protein which harbors three coiled coil domains with two short linkers, termed intramolecular tandem coiled coil (ITCC) and characterize its structural and biochemical behavior in solution. ITCC consists of three coiled coil domains whose sequences are derived from Coil-Ser and its domain swapped dimer. Modifications include positioning E (Glu) residue at "*e*" and K (Lys) at "*g*" positions throughout heptad repeats to enhance ionic interaction among its constituent coiled coil domains. Molecular modeling of ITCC suggests a compact triple helical bundle structure with the second and the third coiled coil domains forming a canonical coiled coil. ITCC exists as a mixture of monomeric and dimeric species in solution. Small-angle X-ray scattering reveals ellipsoidal molecular envelopes for both dimeric and monomeric ITCC in solution. The theoretically modeled structures of ITCC dock well into the envelopes of both species. Higher ionic strength shifts the equilibrium into monomer with apparently more compact structure while secondary structure remains unchanged. Taken together, our results suggest that our designed ITCC is predominantly monomeric structure through the enhanced ionic interactions, and its conformation is affected by the concentration of ionic species in the buffer.

1. Introduction

Coiled coil is a common structural domain found in a wide range of proteins, and characterized by the hydrophobic core and the surrounding electrostatic periphery. Coiled coil has also been implicated in a milieu of biological functions, ranging from transcription to amyloid [1]. The fundamental sequence domain of the coiled coil is a heptad repeat which consists of seven residues with the first ("*a*") and the fourth ("*d*") positions being hydrophobic one, specifically leucine. Coiled coils form amphipathic α-helices and the driving forces to hold those helices together are the hydrophobic interactions among residues in "*a*" and "*d*" positions and surrounding electrostatic ones. Such two major interactions form basis for forming oligomers with monomers containing the coiled coil domain arranged in either parallel or anti-parallel fashion. In addition to biological involvement, coiled coil has served as a model system to understand protein folding and design, the latter being extended to protein-based material development including nanotubes, cages and much more [2].

Designed coiled coils have served as an excellent model system to understand the basic principles of protein folding and stability. Most designed coiled coils feature intermolecular coiled coils, often leading to multiple oligomeric states. One of early examples involves coiled coils derived from yeast transcription factor GCN4. Coiled coil peptide from GCN4 shows parallel dimeric arrangement [3]. However, when buried hydrophobic residues were mutated, those mutant GCN4 peptides form trimers and parallel tetramers [4]. Coil-Ser, which has 29 residues with four heptad repeats, forms anti-parallel trimers or helical bundles [5]. By contrast, fewer cases have been reported to have intramolecular coiled coils. A "coiled coil stem loop" design with 56 residues constituting two helices connected by a stem loop led to a monomeric intramolecular anti-parallel coiled coil [6]. Domain swapped dimer (DSD), and domain swapped aggregates (DSAg) have three helix bundles being held by both intermolecular and intramolecular

* Corresponding author.
E-mail address: sangholee@skku.edu (S. Lee).

http://dx.doi.org/10.1016/j.bbrc.2014.11.013
0006-291X/

interactions: Two helices (domains I and II) are from one polypeptide and the third one (domain III) is from another polypeptide. Redistribution of the "*e*" and "*g*" positions in the heptad repeats presumably drives the topological difference of the starting monomer, which in turn leads to either DSD or DSAg [5,7].

Electrostatic interactions in coiled coil design have served as key regulatory elements to control conformation and oligomeric state of the resulting coiled coils. For instance, a negatively charged 30-residue peptide where E (Glu) occupies the positions "*e*" and "*g*" formed a coiled coil at acidic pH and high salt [8]. A set of 35-residue peptides with K (Lys)–E (Glu) pairs revealed that ionic interactions are critical in forming intra- and inter-helical coiled coil pairs [9]. In this case, salt concentrations modulate protein stability.

We aim to prepare an intramolecular tandem coiled coil (ITCC) which is longer than the coiled coil stem loop so that ITCC can be used as a larger building block in biomaterial construction. Also desired is the property that ITCC could form an oligomer comparable to fibrils in size when necessary, similar to the relationship between DSD and DSAg. To achieve these goals, we construct ITCC containing three coiled coil domains whose sequences are derived from Coil-Ser and DSD. Charged residues in the "*e*" and "*g*" positions are introduced for the purpose of conformational and oligomeric state regulation. We characterize ITCC both structurally and biochemically in solution using combination of molecular modeling, small-angle X-ray scattering, size exclusion chromatography and circular dichroism. Our ITCC construction and characterization will add one more component in the repertoire of coiled coil-based biomaterials.

2. Materials and methods

2.1. Cloning, protein expression and purification

Primers for PCR were chemically synthesized (Table S1). DNA encoding NZIP was first amplified from the NZIP template by the primers NZ-*Nde*I and NZ-*Bam*HI. The amplified DNA was digested with *Nde*I and *Bam*HI, and cloned into the polylinker region of pET28a (Novagen). The resulting plasmid, pNZIP, was used to clone the second NZIP at *Eco*RI and *Hind*III sites. The second NZIP DNA was amplified with NZ-EK and NZ-Hter: the former contains *Eco*RI and *Kpn*I sites at its 5′-end and the latter contains *Hind*III sites at the 3′-end and a termination codon just after the last codon of the NZIP. This second NZIP DNA was cleaved by *Eco*RI and *Hind*III and ligated to the *Eco*RI/*Hind*III-cut pNZIP. The resulting pNZ-NZ contains an extra *Kpn*I site that would be used for next cloning step for CZIP-coding DNA. Finally, DNA coding for CZIP was amplified with CZ-*Bam*HI and CZ-*Kpn*I and subsequently treated with *Bam*HI and *Kpn*I. The enzyme-cleaved CZIP DNA was ligated to the *Bam*HI/*Kpn*I-cut pNZ-NZ plasmid DNA. The final plasmid, pHis-ITCC, contains the N-terminal His-tag followed by NZIP, CZIP and NZIP in order. GSGG and GTGG linkers were placed between the first NZIP and CZIP, and CZIP and the second NZIP for flexibility, respectively.

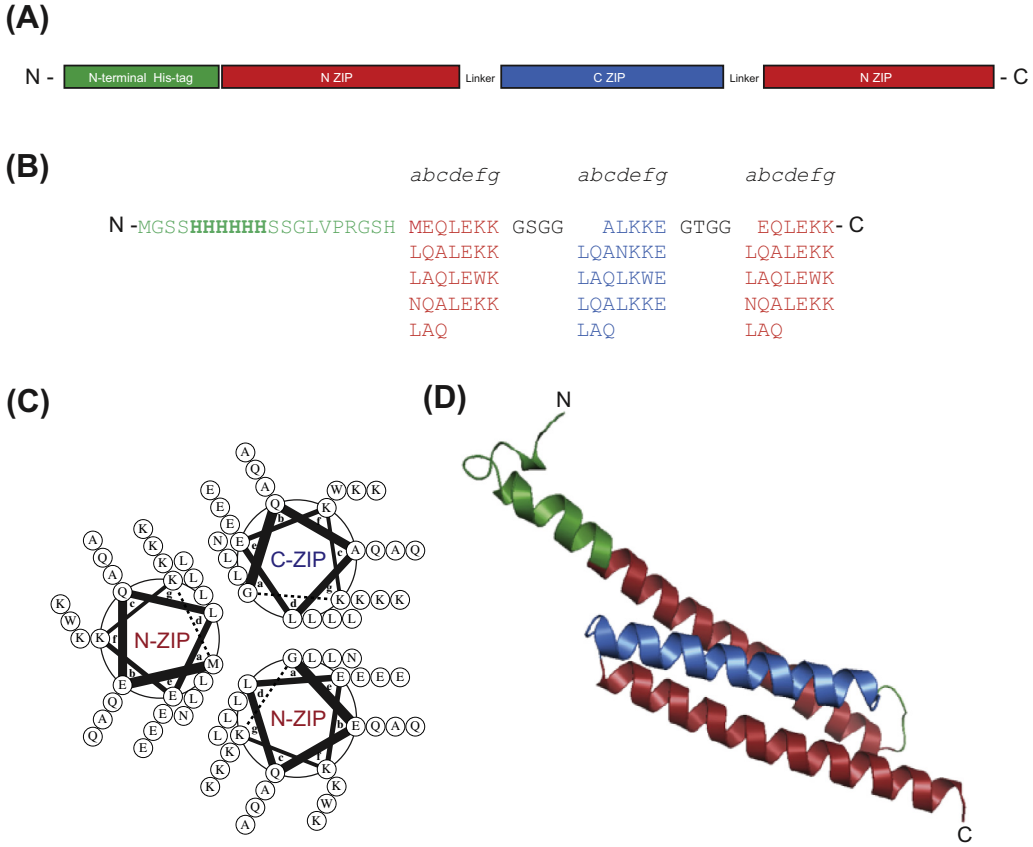

Fig. 1. Sequence and structural model of ITCC. (A) Sequence and domain architecture of the ITCC. N-terminal His-tag is colored green, N-ZIP red, and C-ZIP blue. (B) Primary sequence of the ITCC with the same coloring scheme as in (A). Heptad repeats, $(abcdefg)_n$, shown in columns with positions above. Linker sequence is shown in black. (C) Helical wheel diagram of the ITCC generated by *DrawCoil* [21], Note the perfect pairing of acidic residues (Glu) in the "*e*" position and basic ones (Lys) in the "*g*" position. (D) An *rigid body* model of the monomeric ITCC generated by the Robetta server. Ribbon representation of the model was prepared using PyMOL (Schrödinger). Coloring scheme is the same as in (A). (For interpretation of the references to color in this figure legend, the reader is referred to the web version of this article.)

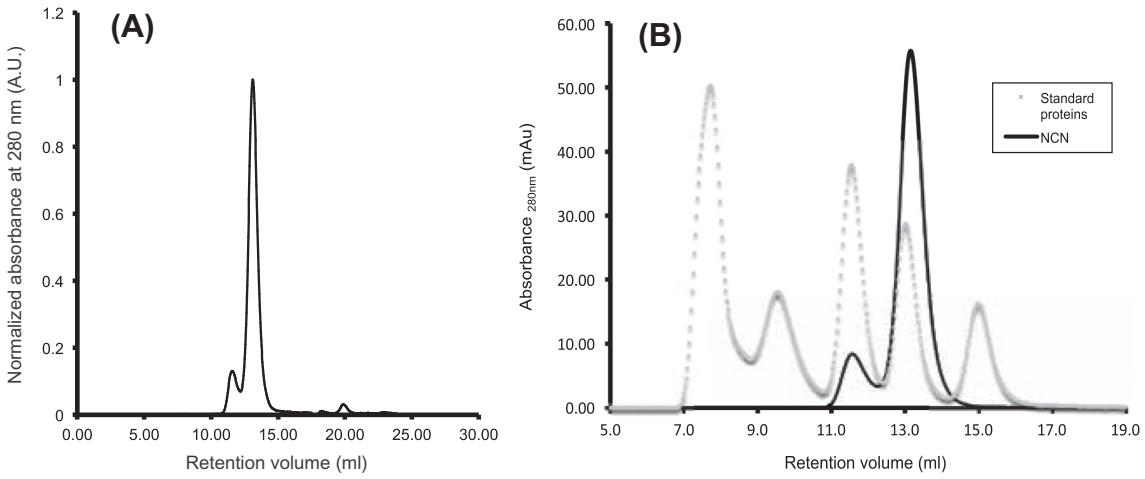

Fig. 2. Biochemical characterization of ITCC by size exclusion chromatography. (A) A representative chromatogram of ITCC on a Superdex 75 10/300 GL column following Ni-NTA affinity chromatography. Two major peaks presumably correspond to monomeric and dimeric species. (B) Calibration curve for molecular mass estimation using protein standards. Protein standards include bovine serum albumin (BSA) (132 kDa; dimer, 66 kDa; monomer), carbonic anhydrase (29 kDa), cytochrome C (12.4 kDa), and aprotinin (6.5 kDa).

His-ITCC was expressed in *Escherichia coli* strain BL21(DE3). Cells were grown at 37 °C until optical density (OD) at 600 nm reached 0.5–0.6, induced with 1 mM (final concentration) isopropyl-β-D-thiogalactoside and further grown at 20 °C overnight. The cells were harvested by centrifugation at 4000 rpm for 20 min. Harvested cells were lysed by sonication in buffer A (50 mM Tris–HCl pH 7.5 and 150 mM NaCl) and the cell lysates were centrifuged at 13,000 rpm for 1 h at 4 °C. The supernatant was applied to a Ni-NTA agarose resin (Qiagen) equilibrated with the buffer A. The proteins were eluted in buffer B (50 mM Tris–HCl pH 7.5, 150 mM NaCl, and 300 mM imidazole). Eluted samples were concentrated and loaded to a Superdex 75 16/60 column (GE Healthcare) pre-equilibrated in the buffer A. Fractions containing ITCC monomer and dimer fractions were pooled separately.

2.2. SEC, DLS, and CD analysis

For analytical size exclusion chromatography, purified ITCC in the buffer A was dialyzed in four buffers with various NaCl concentrations (50 mM Tris HCl pH 7.5 and 1 M/2 M/3 M/4 M NaCl) and loaded to a Superdex 75 10/300 GL column (GE Healthcare) pre-equilibrated with the aforementioned buffers, respectively. A molecular mass calibration curve was constructed using the following standard proteins (Sigma): aprotinin (6.5 kDa), cytochrome c (12.4 kDa), carbonic Anhydrase (29 kDa), and bovine serum albumin (66 kDa). Dynamic light scattering (DLS) measurements were performed on a Dynapro machine (Protein solutions). ITCC protein was pre-incubated in buffer A or four different buffers with various NaCl concentrations (50 mM Tris–HCl pH 7.5 with 1 M/2 M/3 M/4 M NaCl), and its scattering was measured in triplicates. Molecular type of the sample was set to globular protein, and background buffer was set to each of various buffers from parameter options tab in *DYNAMICS* (Protein solution). The stability of ITCC protein was monitored by CD (circular dichroism) at 25 °C. ITCC protein at 17 μM was pre-incubated in the five buffers used for DLS experiments for 30 min. CD spectra were recorded using J-810 CD spectrometer (Jasco) between 230 nm and 320 nm at 1-nm intervals averaged over 2 s.

2.3. SAXS and data processing

ITCC proteins were concentrated to 10 mg/ml using centrifugal concentrator (Millipore) and SAXS data was obtained at CHESS F1 and PAL 4C. Samples were centrifuged for 10 min at 13,000×g before measurements. The buffer A was used for recording reference scattering profile. Each of SAXS profile was collected five times and monitored whether there is radiation damage. To check whether there is concentration dependency, samples were diluted with buffer A (two, five, or ten times), and measured five times. From those original scattering images, 2D Scattering curves were generated by using *BioXTAS RAW* for those data obtained in CHESS and a home-made program for those data from PAL, respectively. *AUTORG* is used to calculate R_g (radius of gyration) and D_{max} from Guinier plot: $I(s) \cong I(0)\exp(-\frac{1}{3}R_g^2q^2)$ [10]. Each of R_g is used to calculate the Pair distribution function ($P(r)$) and Porod volume by *GNOM* [10] for the each scattering profile. Based on ($P(r)$) and Porod volume, molecular envelopes were calculated by *DAMMIF* [11]. To minimize the random error 10 different envelopes were generated, and then these envelopes were averaged using *DAMAVER* [12].

Table 1
Molecular mass estimation of ITCC species.

Technique	Molecular mass (kDa)	
	Monomer	Dimer
Sequence analysis	13.3	26.7
SEC calibration curve	13.8	27.7
DLS analysis	18.6	45.4
SAXS analysis		
Lysozyme standard	14.3	28.1
Absolute $I(0)$	12.9	25.3

2.4. Atomic structure modeling and validation

For the ITCC monomer modeling, five different atomic structural models (M1, M2, M3, M4, and M5) were obtained from Robetta server [13]. Dimer model of ITCC is obtained from *FoXS Dock* that is a method for docking with SAXS profile of the complex. The input files for the *FoXS Dock* are two protein models, and a SAXS profile for the complex [14]. To find the best dimer model that fits the dimer SAXS profile, 5 different combinations of monomer models were used (M1-M1, M2-M2, M3-M3, M4-M4, and M5-M5). To validate those models, *FoXS server* is used to fit each model to SAXS profile, and we selected the best-fitted model to explain molecular envelope based on χ score [14]. Visualization

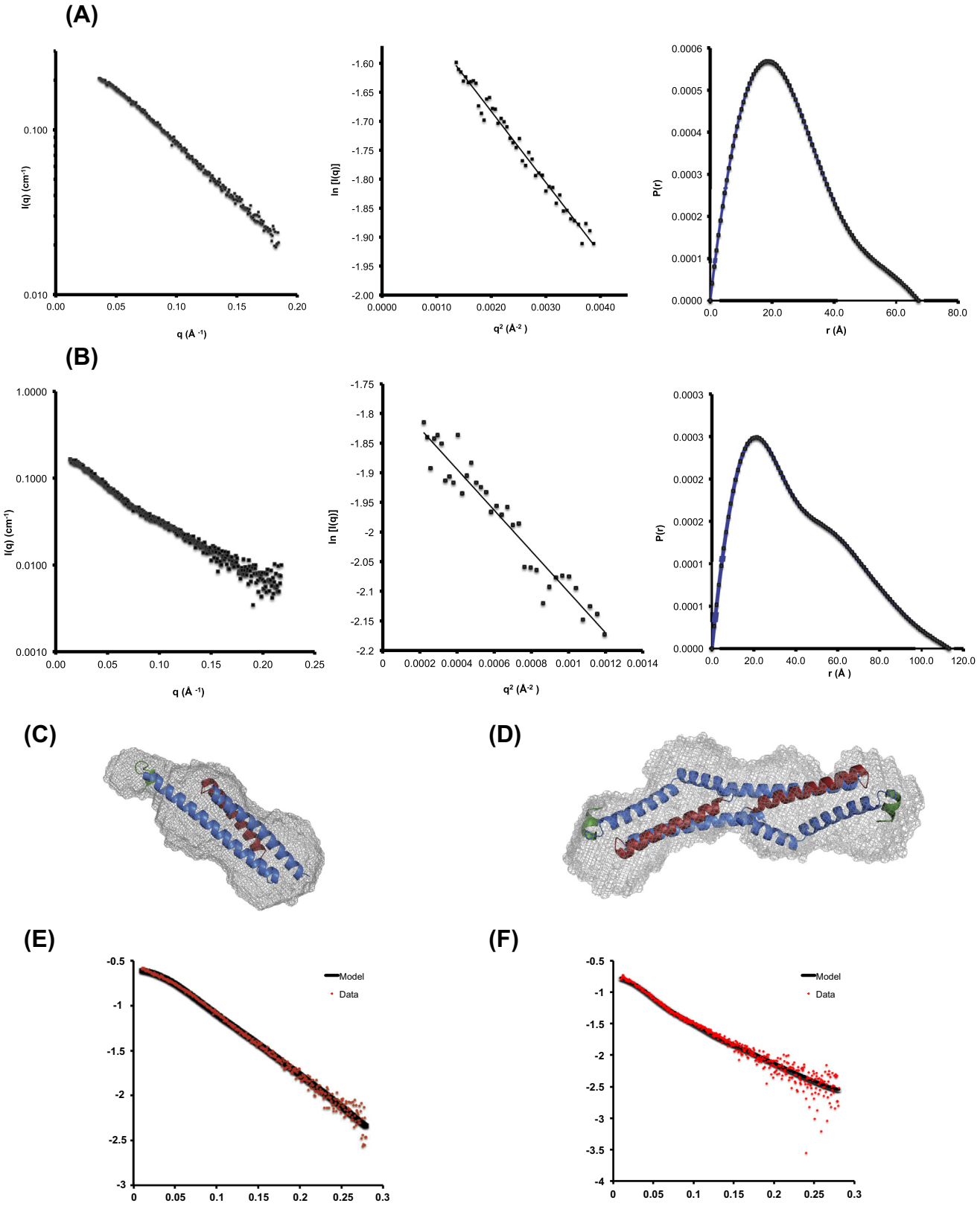

Fig. 3. SAXS data and analysis. (A and B) Raw intensity profiles (left), Guinier plots (middle), and pair distance distribution function plots (right) are shown for the monomer in (A) and the dimer in (B). (C and D) Molecular envelopes (left) and model fitting (right) for the monomer in (C) and the dimer in (D). (E and F) Comparison of experimental data with calculated SAXS profiles of the monomer in (E) and the dimer in (F). SAXS profiles of monomer and dimer models were calculated using *FoXS server*.

and superposition of the modeled structure to the molecular envelope were done by *SUPCOMB* [15], and *PyMOL* (Schrödinger).

3. Results

3.1. Construction and molecular modeling of ITCC

ITCC features three coiled coil domains of two kinds arranged in tandem with short linker sequences (Fig. 1A). The two kinds of coiled coil domains are derived from the sequences of synthetic coiled coils. The first kind (red color in Fig. 1A and B), termed "NZIP", is inspired by a synthetic triple-stranded helical bundle called Coil-Ser (PDB ID: 1COS), and the second one (blue color in Fig. 1A), termed "CZIP", by a domain swapped dimer (DSD; PDB ID: 1G6U) [5,7]. Therefore, ITCC consists of NZIP-CZIP-NZIP. To connect the aforementioned three coiled coil domains, we add two four-residue linkers (G[S/T]GG). The linker sequence is known to be flexible within a designed protein [16,17]. Our ITCC resembles DSD such that both proteins contain multiple coiled coil domains covalently linked in one polypeptide chain. However, ITCC is different from DSD in some aspects. First, each coiled coil domain of ITCC contains four heptad repeats while DSD has two repeats per domain [7]. Secondly, ITCC has charged residue distribution different from DSD: each coiled coil domain has E (Glu) at the entire "*e*" position, and K (Lys) at "*g*". By contrast, each domain of DSD has E (Glu) or K (Lys) at either "*e*" or "*g*" or both positions depending on the domain (Figs. 1, S1 and Table S2). These differences could render ITCC behavior in solution differently from DSD. A structural model for the monomeric ITCC was generated by Robetta server [13]. The ITCC structural model consists of three helices with each corresponding to either NZIP or CZIP connected by two linkers (Fig. 1D). The linker sequences clearly separate three helices for NZIP and CZIP, which is different from DSD in that there is only one linker between the domains I and II, and not between the domains II and III. The introduction of the linker between helices would provide a pivot point around which the connected helices can rearrange to cause conformational changes under appropriate conditions.

3.2. ITCC exists as both monomer and dimer in solution at physiological condition

As the first step in biochemical characterizations of ITCC, we performed size exclusion chromatography to determine solution behavior of ITCC (Fig. 2). Interestingly, chromatogram at physiological condition (pH 7.5, 150 mM NaCl) revealed two peaks, implicating that ITCC exists at least in two different oligomeric states at the physiological condition (Figs. 2A and S2). Calibration curve indicated that the peaks in the chromatogram correspond to monomer and dimer, with 13.81 kDa and 27.73 kDa, respectively (Fig. 2B). Peak integration analysis suggests that the presumably monomeric species accounts for 86.8% while the dimeric one 13.2%. Dynamic light scattering data is consistent with the molecular mass estimates by the calibration curve (Table 1). Using globular protein model, estimated molecular masses for the two peaks are 20.6 and 50.8 kDa, respectively. To obtain independent assessment of oligomeric states of the two peaks, we estimated molecular mass of each peak using small angle X-ray scattering (Table 1). We employed two independent methods for molecular mass estimation: a calibration with a known standard protein (in this case, lysozyme) and a calculation based on absolute scattering intensity $I(0)$ [10]. The molecular mass of the presumably monomeric peak from the size exclusion chromatogram was estimated to be 14.3 and 12.9 kDa, respectively (Table 1). The presumably dimeric peak yielded molecular mass estimate of 28.1 and 25.2 kDa, respectively. Given that the calculated molecular mass values for monomer and dimer are 13.3 and 26.7 kDa, the values obtained by SAXS measurements are fully consistent with the idea that the two peaks from the size exclusion chromatogram correspond to monomer and dimer of ITCC. Taken together, our results establish that ITCC exists as both monomer and dimer at the physiological condition with the monomer being the major species.

3.3. Solution structure of ITCC by small-angle X-ray scattering

To obtain the structural information of the monomer and dimer forms of ITCC, we determined solution structure of ITCC by SAXS (Fig. 3). Monomer and dimer peaks from size exclusion chromatography were pooled separately and subject to data collection (Fig. 3A and B, left panels). Initial measurements at three different concentrations (6.38, 3.19 and 1.28 mg/ml) revealed no concentration effects (Fig. S3 and Table S3). Guinier plot analysis revealed that ITCC is well ordered in solution, enabling us to determine absolute intensity $I(0)$ and the radius of gyration (R_g) values for both species (Fig. 3A and B, middle panels and Table 2). $I(0)$ and R_g values determined by pair distance distribution function, $P(r)$, are consistent with those by the Guinier analysis. D_{max} was calculated from $P(r)$ (Fig. 3A and B, right panels and Table 2). The values for D_{max} are comparable to those calculated from the model structures using *FoXS server* [14,18]: 67.18 Å vs. 67.2 Å (model) for monomer and 113.12 Å vs. 110.63 Å (model) for dimer. Molecular envelopes for both the monomer and the dimer of ITCC were calculated by *DAMMIF* [11]. The *ab initio* model for the ITCC monomer by the Robetta Server (Fig. 1C) fits well into the envelope (Fig. 3C). Inverse Fourier fitting using the ITCC monomer model agrees well with the observed intensities, supported by $\chi = 1.18$ (Fig. 3E) [14,18]. To generate the ITCC dimer model from the SAXS profile, *FoXS Dock* web server was used [19]. It generated a reasonable dimer model from the given ITCC dimer SAXS profile, and two monomer coordinate files. The resulting dimeric model was reasonably fitted into the envelope (Fig. 3D), supported by $\chi = 1.15$ (Fig. 3F) [14,18]. Because of the resolution limitation of SAXS, rigid body model of dimer cannot be obtained at atomic level. However, It is clear that SAXS profile of dimer model has longer D_{max} than monomer (67.18 Å vs. 113.12 Å), and results in elongated molecular envelope.

Table 2
SAXS data collection and analysis statistics.

	Monomer	Dimer
Data-collection parameters		
Synchrotron beamlines	PAL-4C/CHESS-F1	
Beam geometry	Mica window solid cell/oscillation capillary	
Wavelength (Å)	1.24/1.26	
Exposure time (min)		
Concentration range (mg/ml)	0.69–3.47	0.29–1.47
Sample parameters		
Polydispersity (%, by DLS)	6.31	9.11
Structural parameters		
$I(0)$ (cm^{-1}) [from Guinier]	0.238	0.173
R_g (Å) [from Guinier]	19.2 ± 1.1	32.3 ± 4.6
$I(0)$ (cm^{-1}) [from $P(r)$]	0.24	0.17
R_g (Å) [from $P(r)$]	19.93	33.26
D_{max} (Å)	67.18	113.12
Porod volume estimate ($Å^3$)	19934.6	26462.8
Software employed		
Primary data reduction	*RAW*	
Dara processing	*PRIMUS*	
Ab initio analysis	*DAMMIF*	
Validation and averaging	*DAMAVER*	
Three-dimensional representations	*PyMOL*	

3.4. Effects of ionic strengths in the tertiary and the quaternary structures of ITCC

Since ITCC contains perfect pairing of acidic and basic residues in the "*e*" and "*g*" positions and the oligomeric state was obtained experimentally, we pursued how such electrostatic interactions are modulated by ionic strengths, thereby affecting the tertiary and quaternary structures of ITCC. First, we examined size exclusion chromatograms with various NaCl concentrations. Increase in NaCl concentration from 150 mM to 4 M resulted in reduction of the dimeric species and shift of the monomeric species at later retention volume (Fig. 4A). Dimer peaks were observed at 150 mM,

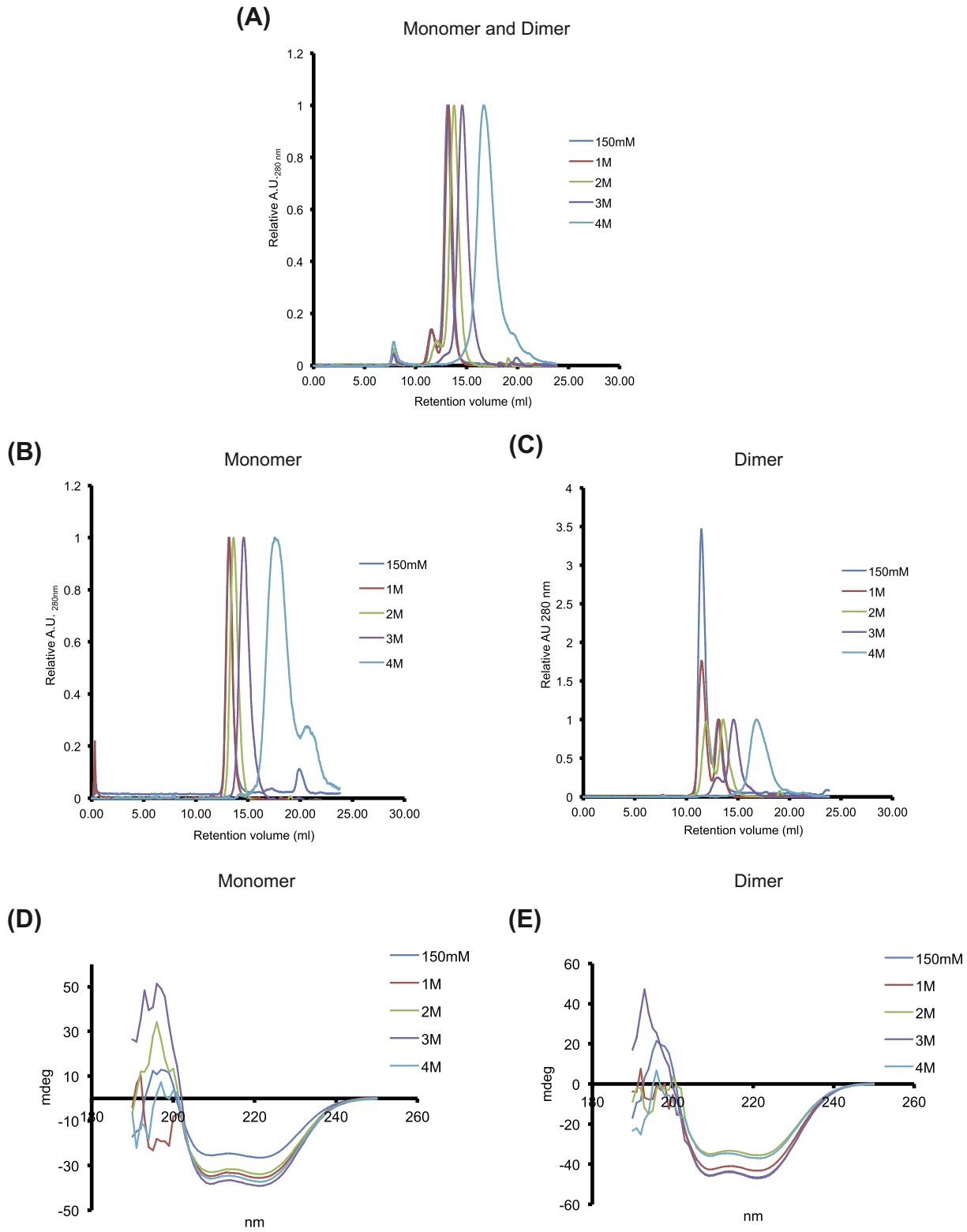

Fig. 4. Effect of ionic strength on the tertiary and quaternary structures of ITCC. (A–C) Size exclusion chromatogram of ITCC at various NaCl concentrations for the monomer and dimer mixture in (A), Monomer in (B), and dimer in (C). (D and E) CD analysis of ITCC at various NaCl concentrations for the monomer in (D), and the dimer in (E).

1 M, and 2 M NaCl concentrations, but disappeared when the concentration increased to 3 M and 4 M NaCl. Such results suggest that under higher ionic strength, ITCC may exist predominantly as a monomer in solution. Furthermore, a peak shift corresponding to the monomer was observed at 3 M and 4 M NaCl concentrations. Apparent monomer peaks were shifted towards later retention volume, implicating that the monomeric structure at 150 mM (Figs. 1C and 3C) may become more compact.

To further analyze the structural changes described above, we attempted to separate monomeric and dimeric species from the initial size exclusion chromatography and investigated the effect of ionic strength separately. The monomeric ITCC clearly showed peak shift to later retention volume (Fig. 4B). To whether the peak shift may have been caused by proteolytic degradation, we analyzed the corresponding fractions from the size exclusion chromatograms by gel electrophoresis (Fig. S2). We observed no sign of proteolytic degradation. These results suggest that the tertiary structure of monomeric ITCC is affected by ionic strength in that higher salt concentrations render ITCC to adopt more compact conformations as a monomer. When the dimeric ITCC was subject to ionic strength increase, the dimeric species apparently dissociated into monomeric one at 3 M and 4 M NaCl concentrations (Fig. 4C).

We then investigated whether higher ionic strength may lead to change in secondary structural contents of ITCC. Circular dichroism spectra of both the monomeric and dimeric ITCC revealed no significant reduction in the helical contents over the NaCl concentrations we tested (150 mM–4 M; Fig. 4D and E). The two characteristic minima at 208 and 222 nm for helical content were maintained in all the samples tested. Taken together, our results establish that ITCC is affected by ionic strength so that higher ionic strength favors monomer over dimer with more compact conformations.

4. Discussion

ITCC exhibits several primary and tertiary structural differences from Coil-Ser, CCSL and DSD. First, ITCC exhibits intramolecular triple helical bundle (Fig. 1D and Table S2) while CCSL contains intramolecular double helical bundle. DSD contains triple helical bundle via both intra-, and inter-molecular interactions. Secondly, ITCC has attractive ionic pairing throughout the entire domains while Coil-Ser has both repulsive and attractive interactions between the coils (2 repulsive and 1 attractive interactions). CCSL forms dimeric intramolecular coiled coil [6] whereas ITCC is predominantly monomeric with a small portion being dimeric. CCSL harbors E (Glu) at "*e*" and "*g*" in entire heptad repeat of the domain I, and K (Lys) for the domain II. Therefore, perfect complementary electrostatic interactions exist between the two domains. However, ITCC possesses E (Glu) residue at "*e*" and K (Lys) at "*g*" in all three domains. Such distribution of charged residues enables CZIP to interact with two NZIPs simultaneously, thereby stabilizing the monomeric species (Fig. 1). Lastly, ITCC contains two linker sequences between its constituent domains. CCSL and DSD contain single linker sequence between the domains I and II. Another designed coiled coil called "sticky-ends coiled coil (SECC) possesses two domains that specifically interact to each other without any linker between them [20]. The presence of two linkers in ITCC seems to enable ITCC to undergo conformational changes by either pH or ionic strength changes, presumably providing more flexibility between the helical domains.

ITCC exists as a mixture of monomeric and dimeric species at physiological condition, which is different from the monomeric CCSL although both ITCC and CCSL are intramolecular coiled coils. Using SAXS, we have modeled the molecular envelope of dimeric and monomeric ITCC in solution. Both species have ellipsoidal shapes, and theoretically modeled structure of ITCC docks well into the envelopes of both ITCC species. Higher ionic strength shifts the equilibrium into monomer with apparently more compact structure. Secondary structure of ITCC at various ionic strengths remains unchanged probed by circular dichroism. Taken together, our results suggest that our designed ITCC is predominantly monomeric structure through the enhanced ionic interactions, and it is affected by the concentration of ionic species in the buffer.

In this study we have constructed an intramolecular coiled coil protein (ITCC) featuring three helical domains connected by two linkers. We investigated the solution behavior of ITCC in different salt conditions. The solution structures of monomeric and dimeric ITCC have been obtained using small-angle X-ray scattering in combination with *ab initio* structural modeling. Increasing ionic strength in the solution apparently drives ITCC to adopt more compact structure in monomeric state while keeping the secondary structural contents invariable. Our data provides a framework by which further protein-based materials can be designed.

Acknowledgments

We thank the staff at the beamlines 4C of Pohang Accelerator Laboratory and F1 of CHESS for technical assistance in collecting SAXS data, and Dr. Kyeong Kyu Kim for access to a CD machine. This work was supported by the National Junior Fellowship (NRF-2011-0001779) to D. Shin., Undergraduate Research Program (2009-04-405, 2010-D-056) through the Korea Foundation for the Advancement of Science and Creativity (KOFAC) to D. Shin and G. Kim., the Rural Development Agency through the Woo Jang Chun Program (PJ009106), and the Pioneer Research Center Program (2012-0009597) through the National Research Foundation of Korea (NRF), funded by the Ministry of Science, ICT and Future Planning to S. Lee.

Appendix A. Supplementary data

Supplementary data associated with this article can be found, in the online version, at http://dx.doi.org/10.1016/j.bbrc.2014.11.013.

References

[1] D.N. Woolfson, The design of coiled-coil structures and assemblies, Adv. Protein Chem. 70 (2005) 79–112.
[2] H. Robson Marsden, A. Kros, Self-assembly of coiled coils in synthetic biology: inspiration and progress, Angew. Chem. Int. Ed. Engl. 49 (2010) 2988–3005.
[3] E.K. O'Shea, J.D. Klemm, P.S. Kim, T. Alber, X-ray structure of the GCN4 leucine zipper, a two-stranded, parallel coiled coil, Science 254 (1991) 539–544.
[4] P.B. Harbury, T. Zhang, P.S. Kim, T. Alber, A switch between two-, three-, and four-stranded coiled coils in GNC4 leucine zipper mutants, Science 262 (1993) 1401–1407.
[5] B. Lovejoy, S. Choe, D. Cascio, D.K. McRorie, W.F. DeGrado, D. Eisenberg, Crystal structure of a synthetic triple-stranded alpha-helical bundle, Science 259 (1993) 1288–1293.
[6] D.G. Myszka, I.M. Chaiken, Design and characterization of an intramolecular antiparallel coiled coil peptide, Biochemistry 33 (1994) 2363–2372.
[7] N.L. Ogihara, G. Ghirlanda, J.W. Bryson, M. Gingery, W.F. DeGrado, D. Eisenberg, Design of three-dimensional domain-swapped dimers and fibrous oligomers, Proc. Natl. Acad. Sci. U.S.A. 98 (2001) 1404–1409.
[8] I. Jelesarov, E. Durr, R.M. Thomas, H.R. Bosshard, Salt effects on hydrophobic interaction and charge screening in the folding of a negatively charged peptide to a coiled coil (Leucine zipper), Biochemistry 37 (1998) 7539–7550.
[9] W.D. Kohn, C.M. Kay, R.S. Hodges, Salt effects on protein stability: two-stranded alpha-helical coiled-coils containing inter- or intrahelical ion pairs, J. Mol. Biol. 267 (1997) 1039–1052.
[10] D. Svergun, Determination of the regularization parameter in indirect-transform methods using perceptual criteria, J. Appl. Crystallogr. 25 (1992) 495–503.
[11] D. Franke, D.I. Svergun, DAMMIF, a program for rapid ab-initio shape determination in small-angle scattering, J. Appl. Crystallogr. 42 (2009) 342–346.
[12] V.V. Volkov, D.I. Svergun, Uniqueness of ab initio shape determination in small-angle scattering, J. Appl. Crystallogr. 36 (2003) 860–864.
[13] D.E. Kim, D. Chivian, D. Baker, Protein structure prediction and analysis using the Robetta server, Nucleic Acids Res. 32 (2004) W526–W531.

[14] D. Schneidman-Duhovny, M. Hammel, A. Sali, FoXS: a web server for rapid computation and fitting of SAXS profiles, Nucleic Acids Res. 38 (2010) W540–544.
[15] M.B. Kozin, D.I. Svergun, Automated matching of high- and low-resolution structural models, J. Appl. Crystallogr. 34 (2001) 33–41.
[16] R. Hjerpe, F. Aillet, F. Lopitz-Otsoa, V. Lang, P. England, M.S. Rodriguez, Efficient protection and isolation of ubiquitylated proteins using tandem ubiquitin-binding entities, EMBO Rep. 10 (2009) 1250–1258.
[17] Y. Jin, M. Zhuang, L.M. Hendershot, ERdj3, a luminal ER DnaJ homologue, binds directly to unfolded proteins in the mammalian ER: identification of critical residues, Biochemistry 48 (2009) 41–49.
[18] D. Schneidman-Duhovny, M. Hammel, J.A. Tainer, A. Sali, Accurate SAXS profile computation and its assessment by contrast variation experiments, Biophys. J. 105 (2013) 962–974.
[19] D. Schneidman-Duhovny, M. Hammel, A. Sali, Macromolecular docking restrained by a small angle X-ray scattering profile, J. Struct. Biol. 173 (2011) 461–471.
[20] M.J. Pandya, G.M. Spooner, M. Sunde, J.R. Thorpe, A. Rodger, D.N. Woolfson, Sticky-end assembly of a designed peptide fiber provides insight into protein fibrillogenesis, Biochemistry 39 (2000) 8728–8734.
[21] G. Grigoryan, A.E. Keating, Structural specificity in coiled-coil interactions, Curr. Opin. Struct. Biol. 18 (2008) 477–483.